

# Laboratory and Model Tests at Reservoir Conditions for CO<sub>2</sub>-Brine-Carbonate Rock Systems Interactions.

Reid B. Grigg, reid@prrc.nmt.edu, Brian J. McPherson, brian@nmt.edu, and Robert K. Svec, bsvec@prrc.nmt.edu, New Mexico Petroleum Recovery Research Center.

SECOND ANNUAL CARBON SEQUESTRATION CONFERENCE, 5-8 May 2003, Washington, D.C.

## Abstract

Determining the viability of, risks in, and optimal locations for sequestering CO<sub>2</sub> in the subsurface requires detailed knowledge of the complex interactions among CO<sub>2</sub>, rock matrix, and pore fluids under appropriate in-situ pressure and temperature conditions. Many physical and chemical processes are known to occur both during and after geologic CO<sub>2</sub> injection, including diagenetic chemical reactions and associated permeability changes. Although it is commonly assumed that CO<sub>2</sub> sequestered in this way will ultimately become mineralized, the rates of these changes, including CO<sub>2</sub> hydration in brines, are known to be relatively slow. Together with hydrated CO<sub>2</sub>, cations from brines may form solid-state carbonate minerals, ostensibly providing permanent sequestration.

Results of a series of laboratory CO<sub>2</sub>-brine flow tests in rock core are being used to calibrate a recently coupled reactive transport simulator, TRANSTOUGH. TRANSTOUGH is a combination of the TOUGH2 simulator, for coupled groundwater/brine and heat flow, with the LANL chemistry code TRANS for chemically reactive transport. This paper presents laboratory test results and compares these to the model predictions. Variability in response among rock types suggests that CO<sub>2</sub> injection will induce ranges of transient and spatially dependent changes in intrinsic rock permeability and porosity. Determining the effect of matrix changes on CO<sub>2</sub> mobility is crucial in evaluating the efficacy and potential environmental implications of storing CO<sub>2</sub> in the subsurface.

## Introduction

This study assesses the viability and environmental implications of sequestering carbon dioxide (CO<sub>2</sub>) in the subsurface. Following injection, some mineral or aqueous trapping may occur,<sup>1</sup> transforming CO<sub>2</sub> into less mobile forms, effectively providing permanent sequestration. However, in-situ pH decreases, dissolution of the rock matrix may occur, increasing permeability and thus, fluid mobility. Inversely, as the fluid proceeds in the reservoir, with the rock becoming saturated and the subsequent pressure decrease reducing solubility in the brine, precipitation may occur. This could result in reduced permeability and CO<sub>2</sub> mobility. Wawersik et al.<sup>1</sup> provide a comprehensive review of science and engineering issues associated with geologic CO<sub>2</sub> sequestration.

Cores of quarried Indiana (Salem) limestone and San Andres dolomite from the Seminole Field in the Permian Basin (Gaines County, Texas) were tested to investigate the relationship between WAG fluids and the formation rock.<sup>2</sup> Pressure transient data was collected for calculation of permeability and injectivity. Core flooding was conducted in the water alternating with gas (WAG) sequence at in-situ conditions. Backscatter electron (BSE) imaging was performed on pre- and post-flood samples to detect changes in the cores. Macroscopic and microscopic dissolution features were observed in all cores exposed to WAG fluids. Carbonate and anhydrite dissolution caused changes in core permeability and porosity.

Work is continuing on further tests on a relatively clean limestone sample. The injected brine has been modified with components that would precipitate as carbonates, but those are not present or are present in low quantities in the limestone. This will aid in quantifying fluid-mineral interactions and the resulting permeability-porosity relationships of this rock type. In this paper, we review the comparison of new tests and previous laboratory work<sup>2</sup> with simulator predictions to evaluate model efficacy.<sup>3</sup>

Injectivity abnormalities in water-alternating-gas (WAG) improved oil recovery (IOR) processes seem to mystify the petroleum industry.<sup>4</sup> A survey conducted by the New Mexico Petroleum Recovery Research Center on CO<sub>2</sub> flooding indicated that loss of injectivity on WAG cycles has been a crucial limiting factor in many projects.<sup>5</sup> Based on the fluid flow properties of CO<sub>2</sub> and other IOR gases, one would intuitively expect that gas injectivity would be greater than the waterflood brine injectivity.<sup>6</sup> However, in practice, this behavior is not always observed. WAG water cycle injectivity has been reported to be higher than the waterflood brine injectivity in several projects (North Ward Estes,<sup>7,8</sup> Mabee,<sup>9</sup> and Cedar Creek Anticline<sup>10,11</sup> projects) and lower in other projects (San Andres Levelland,<sup>12,13,14</sup> Slaughter<sup>13,14</sup> and Wasson Fields<sup>13,14</sup> and a number of gas injection tests<sup>15</sup>). It is perplexing that some reservoirs lose injectivity and others increase injectivity after the first slug of gas (CO<sub>2</sub>) is injected, and that this phenomenon may occur on a local or field wide scale. Injection wells in the same field and reservoir may show significantly dif-

ferent behavior. The change of injectivity has been investigated in the laboratory by several research groups with mixed results.<sup>2,9,16</sup> Change in rock properties due to fluid/rock interactions can account for some of the field injectivity behavior.<sup>17-20</sup>

Studies of CO<sub>2</sub> geologic sequestration remain in the developmental stage, with only a few studies, which are summarized in the following section. Even fewer studies have employed reactive transport simulators; much of this research is proprietary or in developmental stages. Non-reactive transport modeling began in the early 90s when Van der Meer<sup>21</sup> simulated CO<sub>2</sub> sequestration in a circular anticlinal stratigraphic trap. A subsequent study by Holt et al.<sup>22</sup> modified a black oil simulator to include the solubility of CO<sub>2</sub> in H<sub>2</sub>O and incorporated empirical relative permeability relations between liquid and gas phases, both previously not considered by Van der Meer.<sup>21</sup> Their findings indicated that injection rate and absolute permeability were the dominant factors of migration of injected CO<sub>2</sub>. Another study by Van der Meer<sup>23</sup> addressed CO<sub>2</sub> injection into a two-dimensional, quasi-infinite aquifer and concluded that it was possible to sequester significant amounts of CO<sub>2</sub> in the subsurface but added that capturing the combined effects of viscous fingering and gravity segregation would require three-dimensional modeling. Lindeberg<sup>24</sup> described simulations of CO<sub>2</sub> injection in a horizontally finite aquifer. He concluded that CO<sub>2</sub> storage was feasible beneath horizontal seals, provided that injection locations were sufficiently deep.

Law and Bachu<sup>25</sup> conducted a study to simulate multidimensional, multicomponent flow and transport of CO<sub>2</sub> injected into a sedimentary basin for 30 years. This model allows phase partitioning between separate and dissolved phase CO<sub>2</sub>. They concluded that the most important factors affecting CO<sub>2</sub> storage potential include intrinsic permeability and injection pressure, while the unit thickness is moderately important. Weir et al.<sup>26</sup> used the multiphase, multicomponent TOUGH2 model to simulate CO<sub>2</sub> injection in geologic media. They concluded that the most significant factor affecting volumetric CO<sub>2</sub> storage potential is intrinsic permeability. Emulating the work of Weir et al.,<sup>26</sup> Cole<sup>27</sup> added a CO<sub>2</sub> equation of state to the TOUGH2 simulator that incorporated the effect of capillary pressure phenomena. In addition, he changed the previously employed variable-switching technique used in TOUGH2 to a persistent set of primary variables applicable in both saturated and unsaturated conditions. His analyses agreed with previous studies that absolute permeability was the dominant mechanism controlling CO<sub>2</sub> migration and that other significant parameters were the injection rate and injection depth. None of the above studies considered chemical reactions between media, formation fluid, and injected CO<sub>2</sub>.

Johnson et al.<sup>28</sup> used the NUFT<sup>29</sup> simulator package that models the reactive transport of CO<sub>2</sub> injected into geologic media. Simulations were patterned after field scale CO<sub>2</sub> injections that are taking place at Statoil's North Sea Sleipner facility. Their findings indicated that intra-aquifer structures have the most control of separate-phase CO<sub>2</sub> migration paths and solubility within the aquifer unit. In summary, previous work indicates it is possible to sequester CO<sub>2</sub> in the subsurface for long periods under ideal conditions. Previous studies also suggest that absolute permeability of both the aquifer and capping layer are the dominant geologic controls on CO<sub>2</sub> migration.

### Software, Hardware, Procedures, and Simulator

The modeling work covered in this report uses TRANSTOUGH, a simulator that is a combination of three individual modules—TOUGH2,<sup>30</sup> EOSCO2,<sup>27</sup> and TRANS<sup>31</sup>—that have previously been described.<sup>3,32</sup> Briefly, TOUGH-EOSCO2<sup>27</sup> can simulate the flow of mass and energy, including multiphase CO<sub>2</sub>. At the convergence of each time step, execution control is passed from TOUGH-EOSCO2 to TRANS, which then repeats the TOUGH-EOSCO2 time step, simulating the coupled chemical processes at the thermodynamic conditions simulated by TOUGH-EOSCO2. In the present form the modules are sequentially coupled.

All CO<sub>2</sub>-brine injection experiments involve the same basic mechanical configuration discussed in detail in an earlier publication.<sup>2</sup> The laboratory core experiments were simulated using a one-dimensional 100-cell horizontal column with each cell measuring 0.045 cm × 0.045 cm × 0.5 cm. Non-boundary cell volumes were preserved to match the experimental dimensions, but the Dirichlet effluent cell was assigned a larger volume of 1 × 10<sup>6</sup> m<sup>3</sup> to maintain constant boundary conditions for temperature and pressure.

**Rock Characteristics:** Two models were explicitly developed to simulate actual core flow experiments. One was a dolomite-anhydrite system representing San Andres core from the Seminole field in west

Texas. The second was calcite representing quarried limestone. Three other rock types were evaluated in sensitivity analyses to complement the two core flow experiments. The mineralogical volumetric percentages for each media are presented in Table 1. Quartz was chosen for its low reactivity with formation fluids. Evaporite and carbonate mineral fractions within quartz sandstone were chosen to characterize chemical reactivity of lithologically heterogeneous media.

**Table 1. Media Variations Used in the TRANSTOUGH Model Simulations (Porosity 15% for All Except for "A" with a Measured Dolomite-Anhydrite Porosity of 13%)**

A. Dolomite w/ Anhydrite	B. Calcite	C. Quartz	D. Quartz w/ Evaporites	E. Quartz w/ Carbonates
	85% calcite	85% quartz	45% quartz	40% quartz
67% dolomite			20% gypsum	30% calcite
20% anhydrite			20% halite	15% magnesite

The anhydrite mineral fraction in the experimental dolomite-anhydrite rock was estimated to be about 20% by visual inspection of several trimmings from the core stock. The resulting amount of dolomite was calculated as the residual fraction, accounting for the measured porosity.

**Mineral Reaction Kinetics.** In order to determine the influences of varying lithology, fluid-mineral reaction rates were quantified for simulator input. Mineral kinetics in TRANS is calculated as a function of the prescribed kinetic rate constant and mineral surface area, and the degree to which the fluid is in equilibrium with the geologic media. The rate of reaction in TRANS decreases as the system approaches equilibrium and conversely increases as the system diverges from equilibrium.

Reaction kinetics were estimated for calcite in a chemically unsaturated solution using the relationships by Sjöberg and Rickard.<sup>33</sup> An idealized relation to estimate the surface area to volume ratio was used where  $S = (6/D)\lambda$ , in which it is assumed that the effective surface area to volume ratio  $S$  could be approximated by spherical grain particles of diameter  $D$ , corrected for a roughness coefficient  $\lambda$ . The value of  $\lambda$  depends on the degree of weathering, physical mineral properties, and in some cases laboratory preparation.<sup>34</sup> The estimated mean grain size diameter used was 0.1 mm.<sup>35</sup> Using an assumed  $\lambda$  of 1 and  $D$  of 0.1 mm,  $S$  of the calcite media was estimated at 60,000 to 1. The reaction rate constant used for calcite was calculated to be  $\sim 1 \times 10^{-5}$  mol cm<sup>-2</sup> sec<sup>-1</sup>, within an order of magnitude of laboratory values measured at 25°C by Stumm.<sup>36</sup> Since the solubility of calcite decreases as a function of temperature, a lower solubility is expected for higher temperature.

Stumm<sup>36</sup> also measured reaction rates of dolomite and quartz. The dolomite reaction rate constant was measured to be roughly an order of magnitude slower than calcite. The quartz reaction rate constant was reported to be roughly eight orders of magnitude slower than calcite. These relative mineral rate differences were used to estimate the reaction rate constants of dolomite and quartz, relative to the calculated rates of calcite at 38°C. In addition, since the dolomite-anhydrite sample in the experimental system exhibited vugs, the effective surface area of fluid-mineral contact decreased.<sup>34</sup> To account for the decrease in effective surface area, the dolomite reaction kinetics were arbitrarily decreased by an order of magnitude. Therefore, model reaction rate constants for dolomite and quartz were estimated to be  $1 \times 10^{-7}$  mol cm<sup>-2</sup> sec<sup>-1</sup> and  $1.0 \times 10^{-13}$  mol cm<sup>-2</sup> sec<sup>-1</sup>, respectively. However, due to the widely reported difficulties of precipitating dolomite under laboratory conditions,<sup>37,38</sup> dolomite reaction kinetics were deactivated in simulations without an initial dolomite mineral fraction. Lith and Warthmann suggested that dolomite precipitation requires microbial intervention.<sup>39</sup> The TRANSTOUGH simulator predicts dolomite precipitation in a microbe-rich environment, and in laboratory environments (microbe-poor environments) reaction kinetics were deactivated.

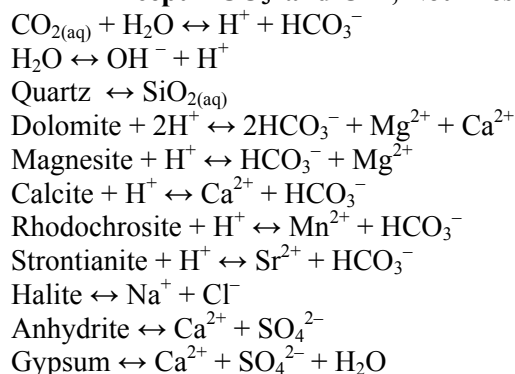
Reaction rate constants for magnesite and dolomite were assumed to be equal. Initial evaporite reaction rates were estimated as an order of magnitude faster than calcite at  $1 \times 10^{-4}$  mol cm<sup>-2</sup> sec<sup>-1</sup>. As with dolomite (in the dolomite-anhydrite sample) the reaction rate of anhydrite was adjusted for preferential flow due to cavities present in the experiment sample. In addition the anhydrite was observed to be concentrated in nodules rather than being dispersed through the sample. The reaction rate was decreased an additional order of magnitude to account for the lower effective reactive surface area of the nodules in relation to a disperse media. Table 2 summarizes the mineral kinetic reaction rate constants used in this

study and example equilibrium constants at 25°C for some of the chemical reactions are listed in Table 3. Equilibria are prescribed through a modified version of a thermodynamic chemical database from Wolery.<sup>40</sup> Homogeneous reactions involving aqueous species were treated as local equilibrium reactions. Therefore CO<sub>2</sub> (aq) and H<sub>2</sub>O instantaneously partition into their associated secondary species at each time step. The described mineral reactions are kinetically driven. This suite of highly simplified aqueous reactions was employed for both the sensitivity analysis and the completed dolomite-anhydrite experiment-model comparison.

**Table 2. Kinetic Reaction Rate Constants**

Mineral	Reaction Rate Constants (mol cm <sup>-2</sup> sec <sup>-1</sup> )	Equilibrium Constants @ 25°C
Halite	$1.0 \times 10^{-4}$	$0.39 \times 10^2$
Gypsum	$1.0 \times 10^{-4}$	$0.33 \times 10^{-4}$
Calcite	$1.0 \times 10^{-5}$	$0.74 \times 10^2$
Anhydrite	$1.0 \times 10^{-6}$	$0.49 \times 10^{-4}$
Dolomite	$1.0 \times 10^{-7}$	$3.26 \times 10^2$
Magnesite	$1.0 \times 10^{-7}$	$1.97 \times 10^2$
Quartz	$1.0 \times 10^{-13}$	$1.00 \times 10^{-4}$

**Table 3. Chemical Reactions Used in the Model (Secondary Species Reactions, Except HCO<sub>3</sub><sup>-</sup> and OH<sup>-</sup>, Not Presented)**



**Brine Composition.** The brine compositions used in most of the laboratory tests and simulations are summarized in Table 4 as concentration “A”. Those listed in “B” are the values used in the last limestone tests using tracer components in the brine. The values in “A” are based on samples of Seminole brine from west Texas.

## Results

**Dolomite-Anhydrite Experiment and Simulations:** In this section TRANSTOUGH simulator predictions are compared to the dolomite-anhydrite experiment results. Input parameters from the experiment are summarized in Column 2 of Table 5. Model predictions were consistent with experimental results, suggesting that the TRANSTOUGH model may be used to simulate subsurface CO<sub>2</sub> injection and its effect on geologic media, at least at the bench-scale and for short time scales. Over the course of the four-month experiment, approximately 145 L of supercritical CO<sub>2</sub> and brine were injected into the dolomite-anhydrite core. Periodically, the core assembly was depressurized and drained in order to measure the porosity of the core sample. Since the core did not need to be depressurized to measure the absolute permeability, measurements were taken when the porosity was measured, and also at several times between porosity measurements. For our analysis, we compared the TRANSTOUGH simulator predictions to ex-

perimental results where both the porosity and permeability were measured (Fig. 1).

**Table 4. Experimental Brine Solution Concentrations**

Brine Component	A. Concentration [M]	B. Concentration [M]
Na <sup>+</sup>	$7.21 \times 10^{-1}$	$1.71 \times 10^{-1}$
SO <sub>4</sub> <sup>2-</sup>	$6.55 \times 10^{-3}$	--
Mg <sup>2+</sup>	$2.60 \times 10^{-2}$	$5.25 \times 10^{-2}$
Cl <sup>-</sup>	$8.46 \times 10^{-1}$	$5.09 \times 10^{-1}$
Ca <sup>2+</sup>	$4.56 \times 10^{-2}$	$4.50 \times 10^{-2}$
Mn <sup>2+</sup>	--	$3.97 \times 10^{-2}$
Sr <sup>2+</sup>	--	$3.15 \times 10^{-2}$

**Table 5. Parameters of the Dolomite-Anhydrite Experiment**

Parameter	Experiment Conditions	Experiment Conditions	Experiment Conditions
Temperature	38°C	38°C	38°C
Back pressure	13.79 MPa	13.79MPa	13.79MPa
Initial saturation	100% Brine A	100% Brine A	100% Tracer Brine B
Geologic media	Rock type A, Table 1	Rock types B-E, Table 1	Rock types A, Table 1
Porosity	13%	15%	15%
Permeability	30.6 mD	38.4 mD	19 mD
CO <sub>2</sub> injection rate	$21.53 \text{ cm}^3 \text{ hr}^{-1}$	$50 \text{ cm}^3 \text{ hr}^{-1}$	$40 \text{ \& } 20 \text{ cm}^3 \text{ hr}^{-1}$
Brine injection rate	$33.09 \text{ cm}^3 \text{ hr}^{-1}$	$50 \text{ cm}^3 \text{ hr}^{-1}$	$40 \text{ \& } 20 \text{ cm}^3 \text{ hr}^{-1}$
Simulated Time	110.9 days	173.6 days	26.3 days

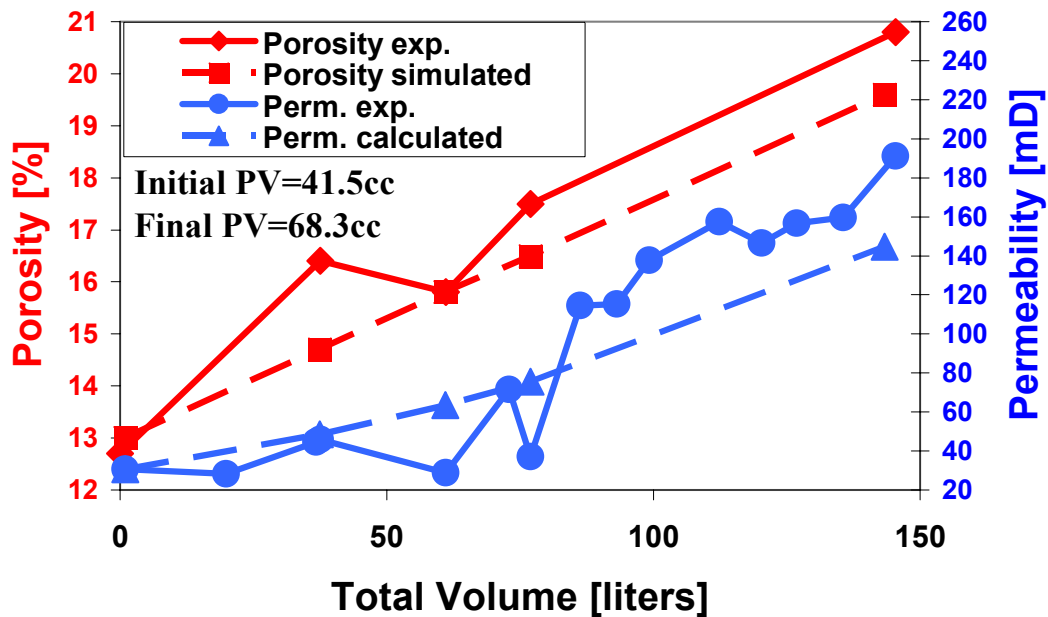


**Fig. 1. Experimental vs. simulated total bulk porosity and permeability values as a function of injected fluid volume.**

The solid lines in Fig. 1 represent the measured porosity and permeability and the dashed lines indicate the values calculated in the TRANSTOUGH model. Model porosity,  $\phi$ , and permeability,  $k$ , were

determined from simulation observations. For example,  $k$  is calculated from porosity where  $k = k_0(\phi/\phi_0)^x$ , and  $k_0$  and  $\phi_0$  are the initial permeability and porosity, respectively, and  $x$  is a fitting exponent. An exponent value of 3.4 was used to calculate the calculated permeabilities plotted in Fig. 1. From the simulated results, bulk permeability was calculated to be a harmonic average of the permeability values from all grid cells. Comparisons are shown as a function of total injected fluid volume. Although there was some attenuation in the simulated response, our comparison revealed strong agreement between TRANSTOUGH simulator predictions and experimental results. The maximum porosity difference between measured and simulated values was always less than 1.5% of the bulk volume, and the permeability differences averaged around 30% of the measured value. Because of the uncertainty in the experimental anhydrite-dolomite volume fraction estimation, the sensitivity to the anhydrite volume fraction amount was examined. The sensitivity of our estimation was tested by simulating a dolomite-anhydrite media comprising 10 and 30% anhydrite volume fractions in addition to our original 20% estimation. The analysis indicated only minor differences in the predicted bulk porosity over time.

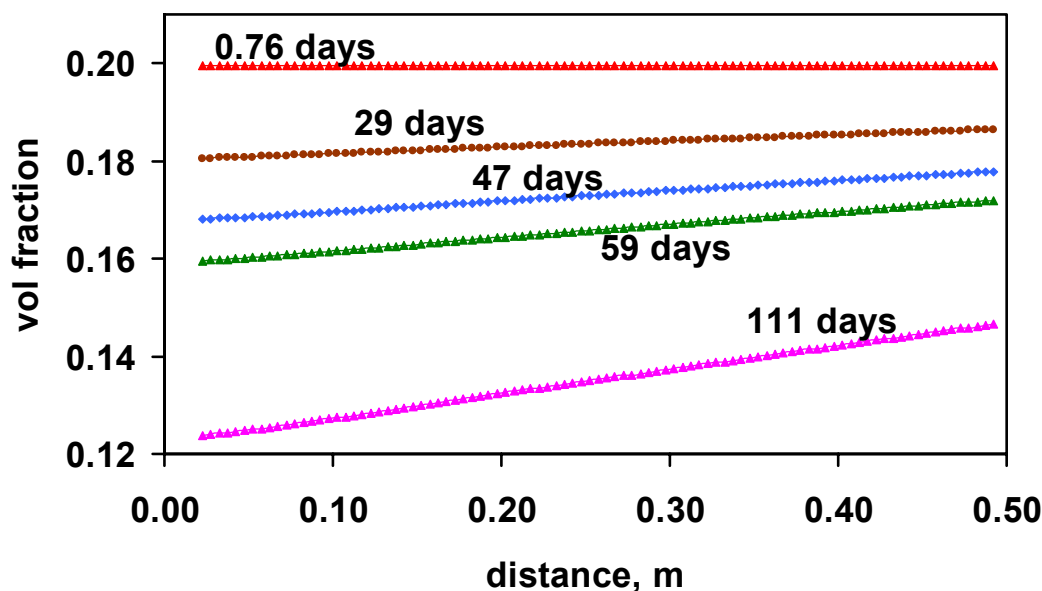


Fig. 2. Volume fraction for anhydrite at selected times indicated in the figure.

The porosity change versus distance along the core plotted in Fig. 1 corresponded with the dissolution of minerals predicted in TRANSTOUGH. Figures 2 through 4 show the simulated volume change of anhydrite, dolomite, and total porosity at five time intervals, respectively, each across the length of the column. About 97% of the volume change was due to anhydrite dissolution over the time frame considered. The slight dolomite dissolution was within a few percentage points of being constant across the column. This is an indication that dissolution was fairly even across the core, thus the solution was significantly undersaturated in dolomite, see Fig. 3. Conversely, examination of Fig. 2 shows that dissolution was uneven across the core, indicating that it is slowed as the solution flowed through the core. This indicates that the system was approaching saturation near enough that dissolution slowed. In the calcite case that will be considered next, the reaction rate was rapid and saturation was reached well within the distance of the core.

Figure 5 is a photo of three cross-sections of the core (injection end, middle and production end) taken after the test was terminated. As predicted, the experimental dissolution occurred across the full length of the core, but increased in extent toward the injection point and decreased as the fluid traveled into the core.

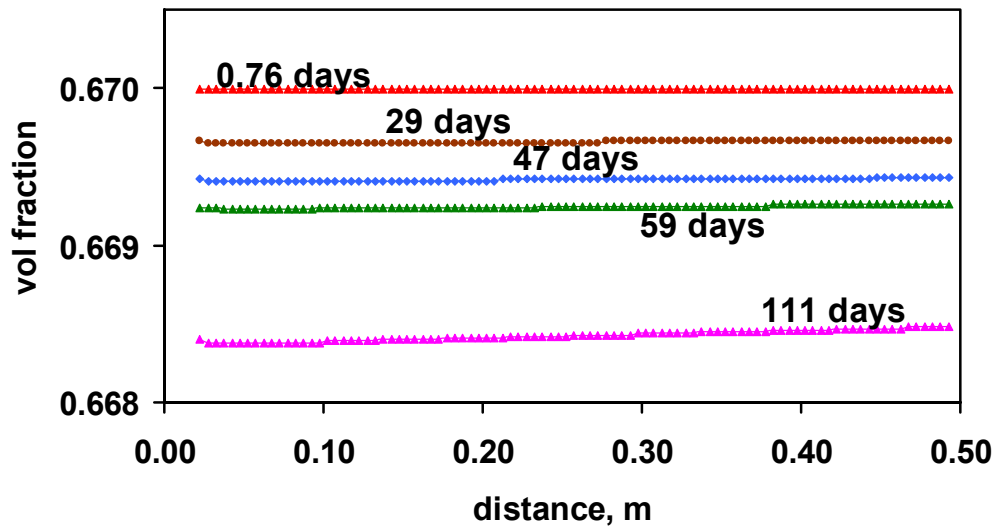


Fig. 3. Volume fraction for dolomite at selected times indicated in the figure.

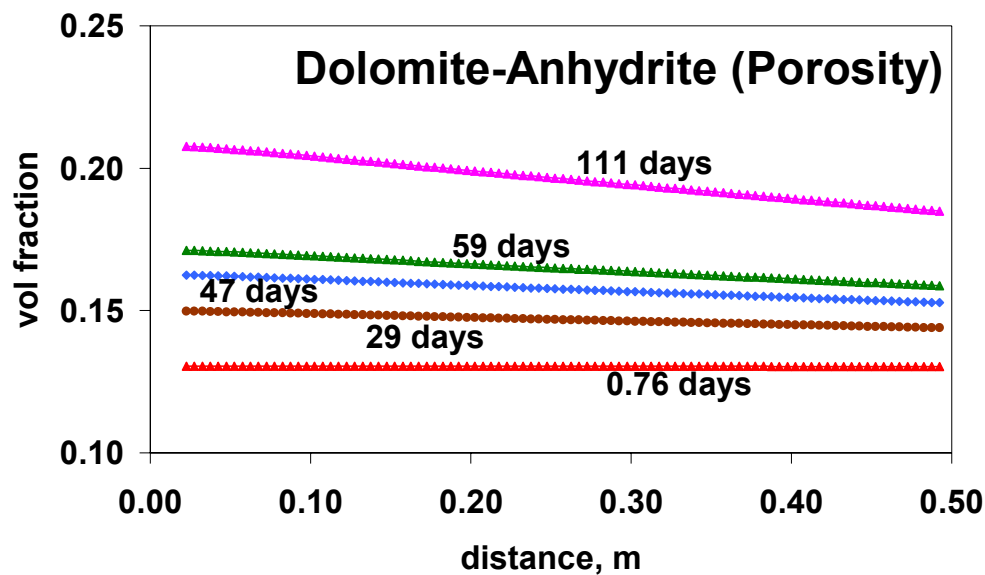
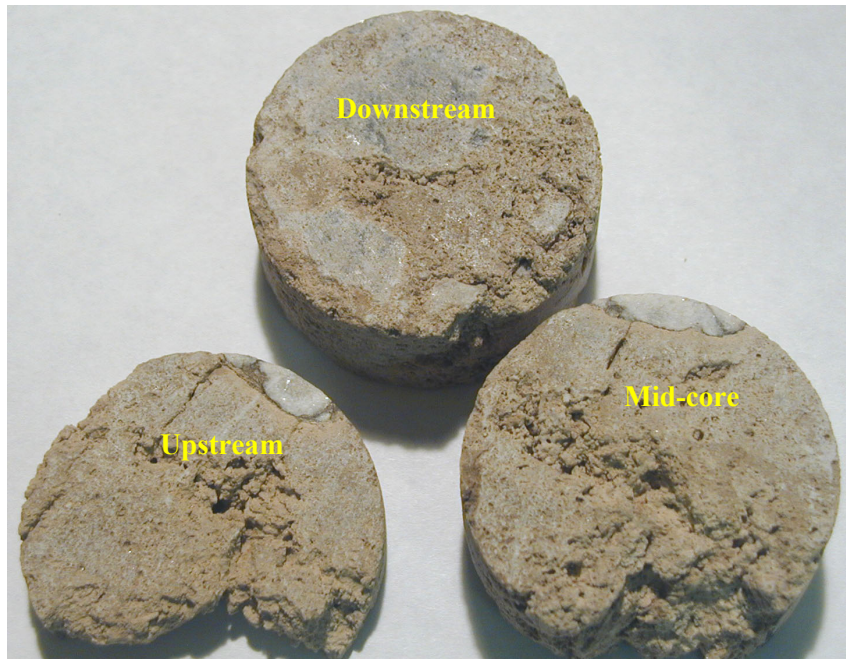


Fig. 4. Porosity volume fraction for the dolomite-anhydrite system at selected times indicated in the figure.

**Simulation of Three Rock Types:** This section discusses the last three systems in Table 1. For these systems, there is no experimental data to compare. The limestone (calcite) systems will be discussed in following sections. These three systems used the parameters listed in Column 3 of Table 2 that also used the Seminole brine solution and the quarried limestone porosity of 15%, core length of about 0.5 m, and tests duration of about 174 days. For the analysis, the response was compared for each media type listed in Table 1, under constant injection of CO<sub>2</sub> and brine.

Simulation results suggest that the pure quartz sandstone was the least reactive media, as expected. Quartz reaction kinetic rates are orders of magnitude slower than most carbonate minerals.<sup>19</sup> As a result, negligible matrix changes were observed over the six-month simulated time scale. CO<sub>2</sub> dissolution in the brine dropped pH from 8.4 to 3.3. All other species concentrations were unaffected by the CO<sub>2</sub> or quartz media and remained constant. Results of the quartz simulations indicate that chemical processes associated with CO<sub>2</sub> and brine injection in pure quartz sandstone are minor.



**Fig. 5. Three cross sections of the San Andres core (injection end, middle, and production end) after the test was completed.**

Contrary to the pure quartz media, the simulated quartz-evaporite sandstone showed significant matrix changes due to  $\text{CO}_2$  and brine injection. As with the pure quartz media, the maximum dissolved  $\text{CO}_2$  was  $\sim 1$  M and the pH decreased to 3.3. At 1.2 days,  $\text{Na}^+$  and  $\text{Cl}^-$  concentrations increased from  $\sim 0.4$  M to approximately 2 M across the column. At the same time,  $\text{SO}_4^{2-}$  and  $\text{Ca}^{2+}$  concentrations doubled across the column. The increase in concentration along the column was likely an indication that fluid flow was fast relative to the mineral reaction rates and brine concentrations. In other words, with smaller Damköhler numbers we expected these concentration increases of chemical species across the column to attenuate. The reason for the disparity in the species concentration is preferential mineral dissolution.

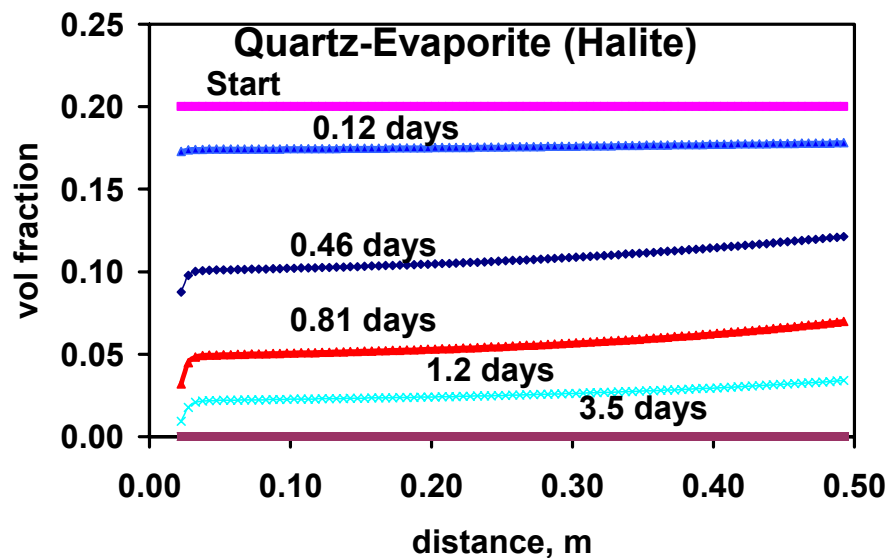


**Fig. 6. Volume fraction of halite versus distance into the column at selected times indicated in the figure.**

Early in the simulation, the majority of the dissolution was from halite. Figure 6 shows that all the halite was dissolved by 3.5 days. By about 88 days all of the evaporite minerals including gypsum had dissolved (Fig. 7). This test demonstrates that significant matrix changes may result on short time scales when both CO<sub>2</sub> and brine fluids are flushed through evaporite rock assemblages. The dissolution of halite was almost even across the column, versus an advancing front for the gypsum. As stated earlier, this is an indication of the fast rate of gypsum dissolution, approaching local equilibrium in a matter of millimeters or centimeters in the core, whereas halite had a relatively slower rate of dissolution compared to achieving local equilibrium as used in the model simulations. These result in a uniform increase in porosity along the length of the column until halite completely dissolves, followed by a sharp front at which porosity increases associated with gypsum. These are shown in Fig. 8 where the total porosity of the system is shown.

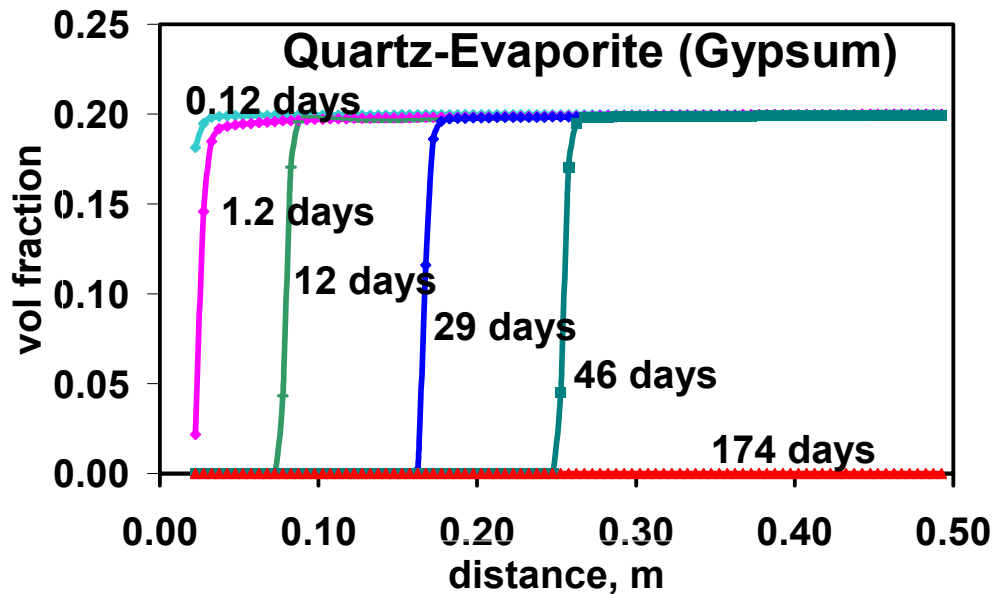


Fig. 7. Volume fraction of gypsum versus distance into the column at selected times indicated in the figure.

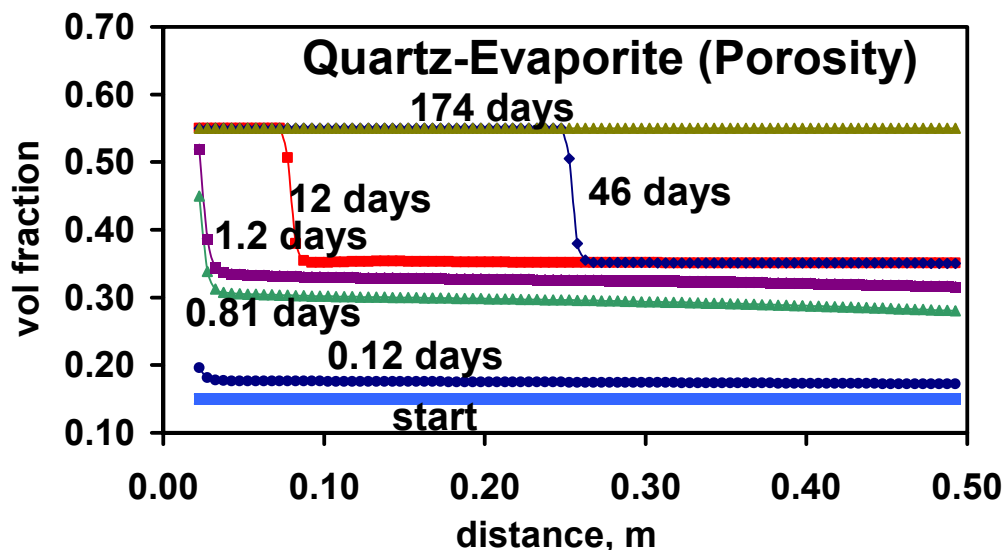


Fig. 8 Porosity volume fraction for the quartz-evaporite system at selected times indicated in the figure.

The quartz-carbonate system had significant but less pronounced dissolution than did the quartz-

evaporite media. In agreement with previous results, the aqueous  $\text{CO}_2$  concentration remained constant at  $\sim 1$  M throughout the simulation. In the initial stages of injection, the brine pH was 5. The cause of the elevated pH was carbonate dissolution, buffering the brine from the effects of  $\text{CO}_2$  acidification.  $\text{Mg}^{2+}$  concentration linearly increased from  $1 \times 10^{-2}$  to  $3 \times 10^{-2}$  M along the column, caused by dissolution of magnesite. In Fig. 9 the volume fraction of magnesite is shown as a function of distance along the column for different times. Only about 5% of the magnesite remained when the simulation was terminated. Calcite dissolved near the injection point, where it was undersaturated due to the acidic conditions, and reprecipitated further along the column as the pH increased and pressure decreased, resulting in an oversaturated system. At 174 days the carbonates were nearly dissolved, which reduced the buffering of the brine solution. As a result pH was held at  $\sim 3.8$  from 0.0 to 0.4 m along the column.

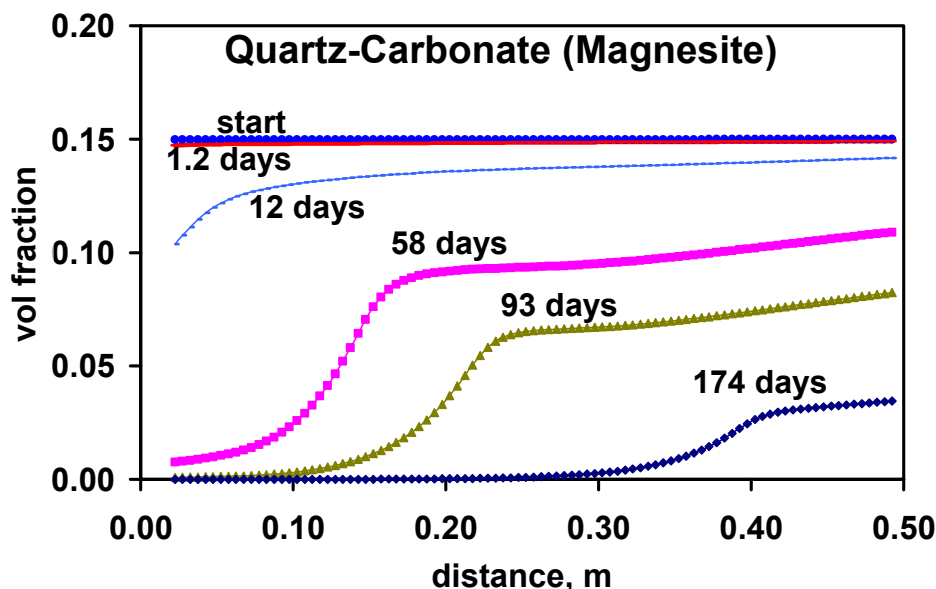


Fig. 9. Volume fraction magnesite versus distance into the column at selected times indicated in the figure.

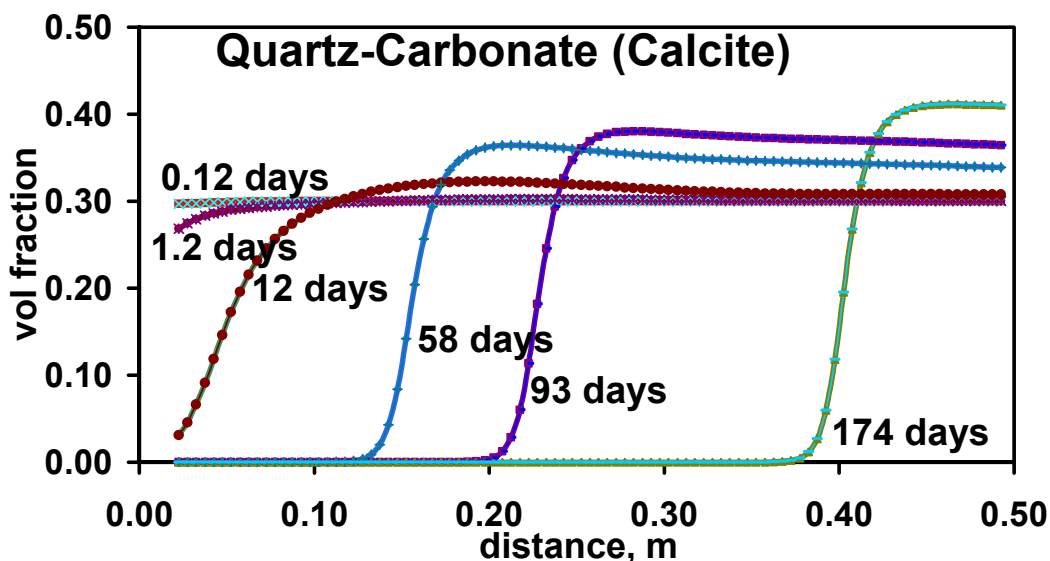


Fig. 10. Volume fraction calcite versus distance into the column at selected times indicated in the figure.

At 0.4 m into the column significant calcite remained (Fig. 10) at the end of the simulation and the solution pH had increased back up to  $\sim 5$ . However, unlike the models of other media, this model predicted calcite mineralization of approximately 0.1 volume fraction from 0.4 m to 0.5 m along the column. This

mineralization could be seen throughout the simulation, increasing with time at the end of the column. If such a phenomenon does indeed occur, it may benefit CO<sub>2</sub> sequestration in two ways. First, dissolution near the injection site may increase storage capacity within the medium, increasing localized CO<sub>2</sub> storage. Second, mineralization may act to reduce the matrix permeability and subsequently CO<sub>2</sub> mobility near the outer boundaries of the main plume. In tandem, dissolving the matrix should increase local storage, whereupon carbonate species within the flushed brine solution precipitate at some downstream location. In this manner, CO<sub>2</sub> injection may act as a self-sealing mechanism. However, in this simulation only 5% of the dissolved carbonates re-precipitated at the tail end of the column.

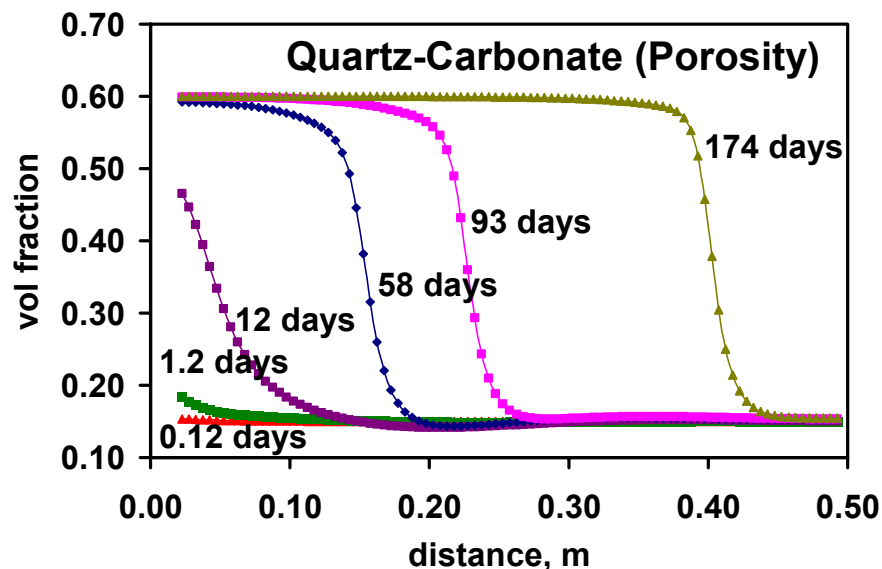


Fig. 11. Porosity volume fraction for the quartz-carbonate system at selected times indicated in the figure.

In an improved oil recovery scenario this deposit could reduce permeability and injectivity, as well as mobility. If our bench scale simulation were representative of a basin scale response, the amount of CO<sub>2</sub> flushing required to seal the media would preclude it as a viable mechanism to reduce permeability. However, if dissolution and subsequent precipitation create concentric sealing layers around the injection location, significant sealing potential may result. In summary, the results suggest that carbonate minerals within quartz sandstone show significant dissolution in CO<sub>2</sub> acidified brine, and that near injection dissolution may induce downstream carbonate precipitation. Figure 11 shows the combined porosity changes from the dissolution and precipitation of the carbonate system. The combined effect is a slight reduction in the porosity ahead of the dissolution then a significant increase in the porosity.

**First Limestone Test and Simulations:** The calcite simulations revealed the same magnitude of dissolution as the quartz-carbonate system (Fig. 12). This simulated a test done in the laboratory on quarried Indiana limestone.<sup>3</sup> The fluid injection rates were identical in each simulation, but the reactive volume fraction (considering quartz as essentially nonreactive) was 2.22 times greater in the pure calcite media. Therefore, if the dissolution was purely a function of the reactive media we should have observed greater matrix changes due to the larger reactive surface of the pure calcite media. However, this was not the case. Increasing the reactive surface area (pure calcite) had little effect on the bulk dissolution, prompting the conclusion that there must be a minimum mineral volume below which decreasing mineral fractions will alter chemical processes. The same effect was observed in the dolomite-anhydrite experiment, where simulations of varying mineral fractions produced similar magnitudes of mineral dissolution. The porosity change is the inverse of the calcite change.

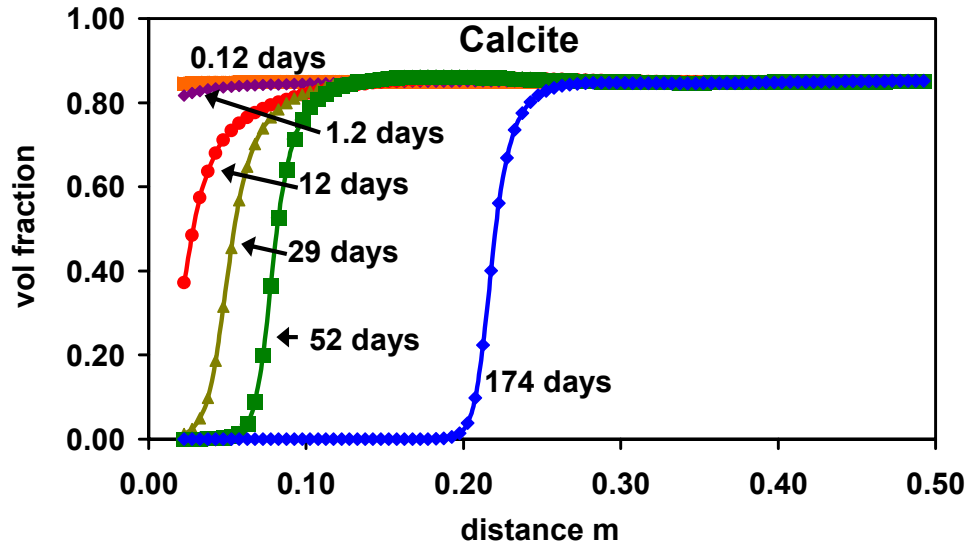


Fig. 12. Volume fraction of calcite versus distance into the column at selected times indicated in the figure.

As in the quartz-carbonate system, calcite showed evidence of mineralization downstream from the dissolution, but it was not as pronounced as that in the previous test shown in Fig. 10. It amounted to about a 1% decrease in porosity ahead of the dissolution channel. Results of the laboratory test on limestone included a solution channel that caused the test to fail at 174 days; these are evident in the photo shown in Fig. 13. This occurrence was discussed in more detail in an earlier paper that included evidence of mineralization downstream, in advance of the solution channel shown in Fig. 13.<sup>2</sup>

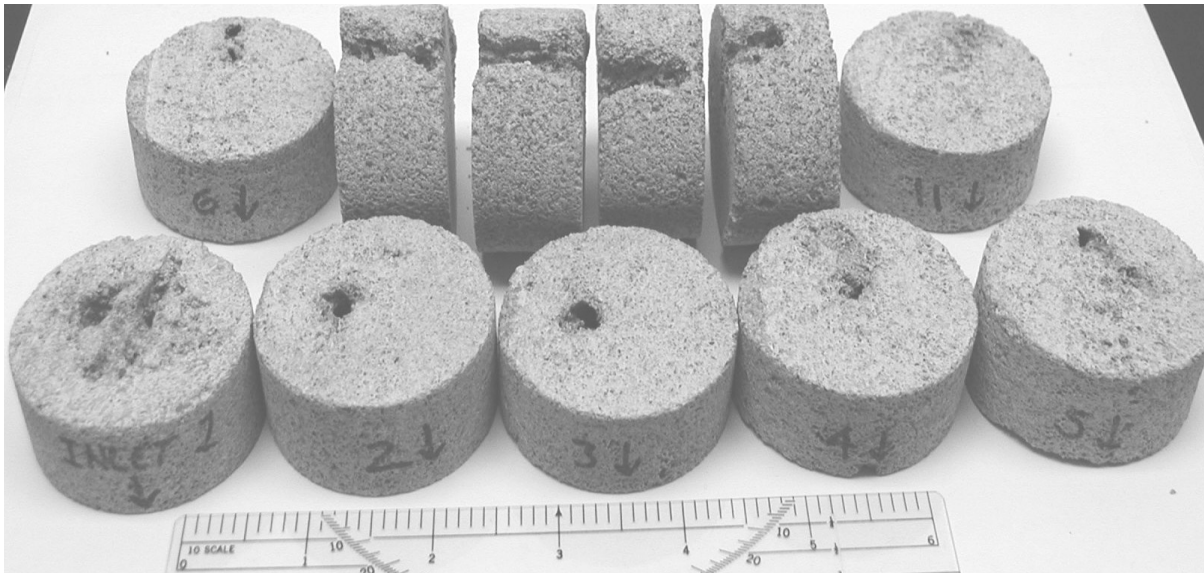


Fig. 13. Limestone after extensive CO<sub>2</sub> and brine injection. Note the solution channel that extended halfway through the core before it failed.

**Tracer-Brine Limestone System Experiment:** In the earlier paper<sup>2</sup> dissolution could be seen on the macroscopic as well as microscopic scale. Precipitation downstream was evident from increased permeability and what appeared to be fresh deposits viewed using the BSE. The deposits had similar composition and structure to the original carbonates and thus the evidence was not conclusive. In this work manganese and strontium chlorides were added to the brine. Manganese and strontium are found in low ppm

concentrations in the limestone. The brine total dissolved solids are given in Table 4, Column 3 under "B". The manganese carbonate, rhodochrosite, and strontium carbonate, strontianite, respectively, are more and less soluble in brine than is calcite. The intent is that, as the brine becomes saturated with carbonate, the precipitant will have a composition different than the pre-flood limestone.

**Table 6. Dimensions of the limestone using brine with tracers.**

	Diameter, cm	Length, cm	Porosity, %
<b>Segment A</b>	<b>5.03</b>	<b>17.15</b>	<b>16.91</b>
<b>Segment B</b>	<b>5.03</b>	<b>39.37</b>	<b>17.54</b>
<b>Entire Core</b>	<b>5.03</b>	<b>56.52</b>	<b>17.35</b>

In this procedure two core samples were selected to be run in series. Table 6 lists the pre-flood core parameters of Segments A and B and Table 6 lists the core parameters. The cores were flooding in series with Segment A first and input and output flow as indicated in the figure. During the flood each segment was removed periodically for porosity and permeability measurements. Figure 14 shows the change in porosity and permeability with time. Due to system problems, porosity at the first of the flood was not obtained for Segments A and B separately. The porosity and permeability of the system as a whole decreased at first, and then increased above the original value by the end of the flood. For Segment A the porosity and permeability became much higher by the end of the tests. A solution channel developed in Segment A. The evolution of the solution channel entrance at three time intervals represented by pore volumes (PV) injected can be seen on the injection face of Segment A.

Figure 15 shows Segments A and B cut longitudinally to show the dissolution of both sections. The solution channel advanced most of the distance across Segment A. The start of some apparent dissolution is seen near the injection face of Segment B. The permeability was becoming high in Segment A and some dissolution was starting in Segment B when the test was terminated. Analysis of the rock samples found increased amounts of manganese and strontium in the core. Figure 16 is a plot of the quantity by weight versus distance across the cores of these two components. Samples were taken every five cm. These show no deposits of chlorides and identify the deposition as carbonates. Manganese levels are increased across the core from less than 100 ppm in fresh core to at least several hundred throughout the flooded core with a peak of 50,000 ppm at 15 cm near the end of the solution channel. Strontium had a similar increase, but not as dramatic. The increase was from a background of about 220 ppm to a peak of 500 ppm at 15 cm into the flood. All the values in the flood were higher and outside one standard deviation of the average fresh core value. More details and additional analysis will be found in a paper that is in press.<sup>41</sup> These results will be used in the future to further test the model TRANSTOUGH.

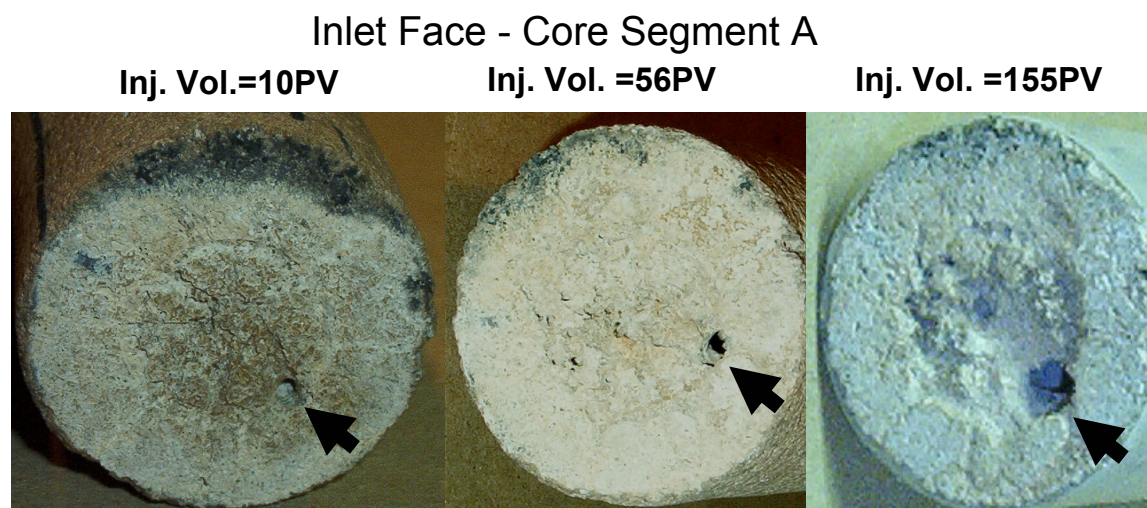


Fig. 14. Development of the solution channel at the injection face of Segment A.

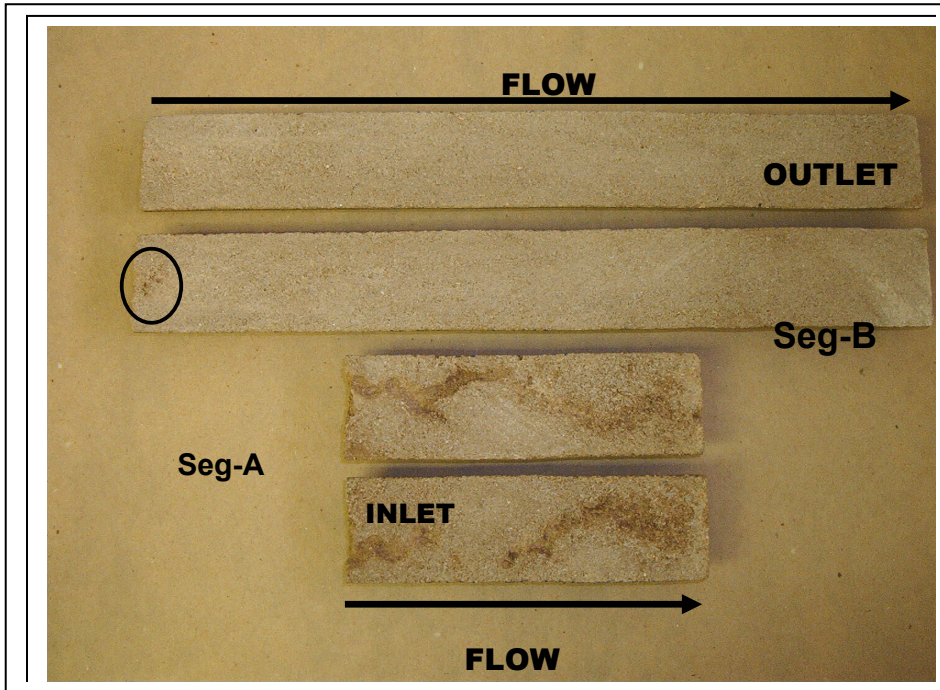


Fig. 15. Two segments of limestone after flooding used in the tracer brine tests.

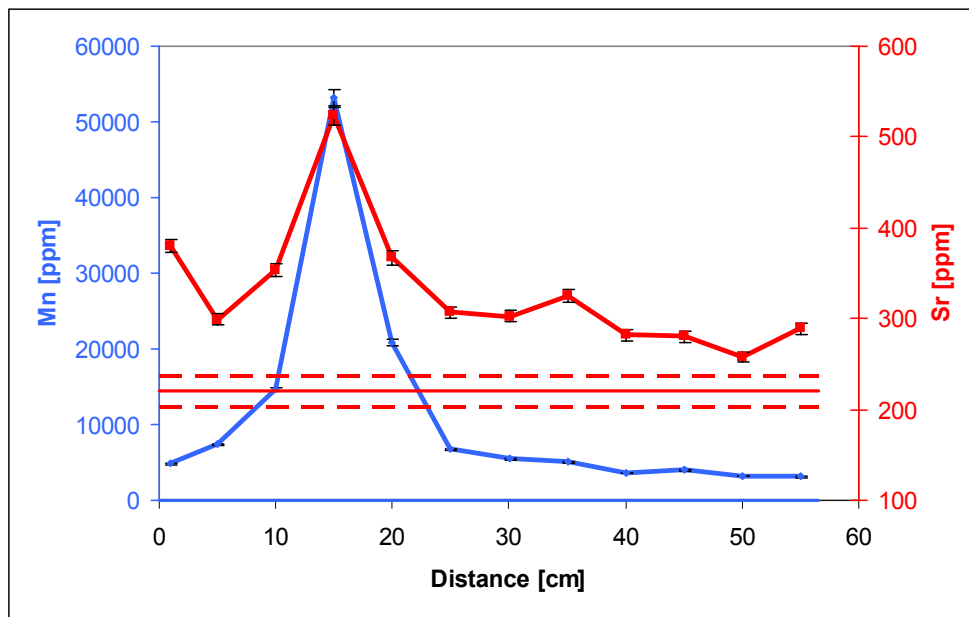


Fig. 16 Composition of manganese and strontium along the core length at the end of the flood.

### Summary

The TRANSTOUGH model was shown to quantitatively replicate the outcome of the dolomite-anhydrite and the limestone, CO<sub>2</sub> and brine injection experiments. The major controlling influence was found to be lithology type, while in the case of the quartz-evaporite media, dissolution may be time-dependent. A secondary influence was the magnitude of fluid flushed through the media in relation to the reactive surface area. Although the TRANSTOUGH model remains in the developmental stages, simulated results

compared favorably to experimental results, suggesting that the model could accurately simulate CO<sub>2</sub> sequestration under known conditions. As bench scale simulations and laboratory experiments are a necessary first step to better characterization of CO<sub>2</sub>-brine-media interactions, reservoir-scale simulations are critical in gaining an understanding of the more applicable large scale effects of heterogeneities that may be incurred from CO<sub>2</sub> injection.

Laboratory tests show that dissolution does occur and that at least some carbonates can precipitate in a relatively short distance. Dissolution and precipitation can be detected from porosity, permeability, and compositional changes in the reservoir rock. The addition of tracers in the brine that could deposit as carbonates that are not in the original core were successfully tested. Both in the laboratory tests and the simulation model, deposition of dissolved carbonates in a saturated solution seem to create a deposition bank at the leading edge of the solution channel.

### Acknowledgement

The authors acknowledge the support of the US Department of Energy (contract no. DE-FC26-01BC-15364) and the State of New Mexico.

### References

1. Wawersik, R., W., et al.: "Terrestrial Sequestration of CO<sub>2</sub>: An Assessment of Research Needs," *Advances in Geophysics* **43**, (2001).
2. Svec, R.K. and Grigg, R.B.: "Physical Effects of WAG Fluids on Carbonate Core Plugs," paper SPE 71496 presented at the 2001 SPE Annual Technical Conference and Exhibition, New Orleans, Sept. 30–October 3.
3. Wellman, T.P, Grigg, R.B., McPherson, B.J., Svec, R.K., and Lichtner, P.C.: "Evaluation of CO<sub>2</sub>-Brine-Reservoir Rock Interaction with Laboratory Flow Tests and Reactive Transport Modeling," paper SPE 80228 presented at the 2003 SPE Oilfield Chemistry Symposium, Houston, February 5-8.
4. Rogers, J. D. and Grigg, R.B.: "A Literature Analysis of the WAG Injectivity Abnormalities in the CO<sub>2</sub> Process," *SPEEE*, October 2001, 375-386.
5. Grigg, R.B. and Schechter, D.S.: "State of the Industry in CO<sub>2</sub> Floods," paper SPE 38849 presented at the 1997 SPE Annual Technical Conference and Exhibition, San Antonio, Oct. 6-9.
6. Hadlow, R.E.: "Update of Industry Experience with CO<sub>2</sub> Injection," paper SPE 24928 presented at the 1992 SPE Annual Technical Conference and Exhibition, Washington D.C., Oct. 4-7.
7. Winzinger, R., *et al.*: "Design of a Major CO<sub>2</sub> Flood, North Ward Estes Field, Ward County, Texas," *SPEEE* (February 1991) 11.
8. Ring, J.N. and Smith, D.J.: "An Overview of the North Ward Estes CO<sub>2</sub> Flood," paper SPE 30729 presented at the 1995 SPE Annual Technical Conference and Exhibition, Dallas, Oct. 22-25.
9. Prieditis, J., et al.: "A Laboratory and Field Injectivity Study: CO<sub>2</sub> WAG in the San Andres Formation of West Texas," paper 22653 presented at the 1991 SPE Annual Technical Conference and Exhibition, Dallas, Oct. 6-9.
10. Christman, P.G., and Gorell, S. B.: "A Comparison of Laboratory and Field-Observed CO<sub>2</sub> Tertiary Injectivity," paper SPE 17335 presented at the 1988 SPE/DOE Enhanced Oil Recovery Symposium, Tulsa, April 17-20.
11. Good, P.A. and Downer, D.G.: "Cedar Creek Anticline Carbon Dioxide Injectivity Test: Design, Implementation, and Analysis," paper SPE 17326 presented at the 1988 SPE/DOE Enhanced Oil Recovery Symposium, Tulsa, April 17-20.
12. Henry, R.L., et al.: "Utilization of Composition Observation Wells in a West Texas CO<sub>2</sub> Pilot Flood," paper SPE 9786 presented at the 1981 SPE/DOE Enhanced Oil Recovery Symposium, Tulsa, April 5-8.
13. Patel, P.D., et al.: "An Investigation of Unexpectedly Low Field-Observed Fluid Mobilities During Some CO<sub>2</sub> Tertiary Floods," paper SPE 14308 presented at the 1985 SPE Annual Technical Conference and Exhibition, Las Vegas, Sept. 22-25.
14. Potter, G.F.: "The Effects of CO<sub>2</sub> Flooding on Wettability of West Texas Dolomitic Formations," paper SPE 16716 presented at the 1987 SPE Annual Technical Conference and Exhibition, Dallas, Sept. 27-30.

15. Schneider, F.N., and Owens, W. W.: "Relative Permeability Studies of Gas-Water Flow Following Solvent Injection in Carbonate Rocks," *SPEJ* (Feb. 1976) 23.
16. Kamath J., Nakagawa, F.M., Boyer, R.E., and Edwards, K.A.: "Laboratory Investigation of Injectivity Losses during WAG in West Texas Dolomites," paper SPE 39791 presented at the 1998 SPE Permian Basin Oil and Gas Recovery Conference, Midland, March 25-27.
17. Ross, G.D., et al.: "The Dissolution Effects of CO<sub>2</sub>-Brine Systems on the Permeability of U.K. and North Sea Calcareous Sandstones," paper SPE/DOE 10685 presented at the 1982 SPE/DOE Symposium on Enhanced Oil Recovery, Tulsa, April 4-7.
18. Mathis, R.L. and Sears, S.O.: "Effect of CO<sub>2</sub> Flooding on Dolomite Reservoir Rock, Denver Unit Wasson (San Andres) Field," paper SPE 13132 presented at the 1984 SPE Annual Technical Conference and Exhibition, Houston, Sept. 16-19.
19. Sayegh, S.G., et al.: "Rock/Fluid Interactions of Carbonated Brines in a Sandstone Reservoir: Pembina Cardium, Alberta, Canada," *SPEFE* (December 1990) 399.
20. Bowker, K.A. and Shuler, P.J.: "Carbon Dioxide Injection and Resultant Alteration of the Weber Sandstone, Rangely Field, Colorado," *The American Association of Petroleum Geologists Bulletin*, V. 75, No. 9 (September 1991) 1489.
21. Van Der Meer, L. G. H.: "The Conditions Limiting CO<sub>2</sub> Storage in Aquifers," *Ener. Convers. Mgmt.*, (1993) **34** (9-11), 959-966.
22. Holt, T., I., et al.: "Underground Storage of CO<sub>2</sub> in Aquifers and Oil Reservoirs," *Ener. Convers. Mgmt.* (1995), **36**, 535-538.
23. Van Der Meer, L. G. H.: "The CO<sub>2</sub> Storage Efficiency of Aquifers," *Ener. Convers. Mgmt.* (1995), **36** (6-9), 513-518.
24. Lindeburg, E.: "Escape of CO<sub>2</sub> from Large Horizontal Aquifers Confined Only by a Cap Seal," Conference: Greenhouse Gases: Mitigation Options (1995).
25. Law, H. S. and Bachu, S.: "Hydrological and Numerical Analysis of CO<sub>2</sub> disposal in deep aquifer systems in the Alberta sedimentary basin." *Ener. Convers. Mgmt.* (1966), **37**(6-8), 1167-1174.
26. Weir, G. J., et al.: "Reservoir Storage and Contaminant of Greenhouse Gases," *Transport in porous media* (1996) **23**, 37-60.
27. Cole, B. S.: "An Equation of State for Multiphase CO<sub>2</sub> and Water," Independent Study (M.Sc), New Mexico Institute of Mining and Technology, (1999).
28. Johnson, J. W., et al.: "Reactive Transport Modeling of Subsurface CO<sub>2</sub> Sequestration: Identification of Optimal Target Reservoirs and Evaluation of Performance Based on Geochemical, Hydrologic, and Structural Constraints," *Energex*, (2000).
29. Nitao, J.J.: *Reference Manual for the NUFT Flow and Transport Code, version 2.0*, (1998), Lawrence Livermore National Laboratory, UCRL-MA-130651, 55.
30. Pruess, K.: "TOUGH2- a General-Purpose Numerical Simulator for Multiphase Fluid and Heat Flow," Lawrence-Berkeley Laboratory, (1999).
31. Lichtner, P.C. (2001) *FLOTRAN: User's Manual*, Los Alamos National Laboratory report, LA-UR-02-2349.
32. Wellman, T.P.: *Concatenation of Reactive Transport Model to Simulate CO<sub>2</sub> Sequestration in Geologic Media*, Thesis, New Mexico Institute of Mining and Technology, (2002).
33. Sjoberg, E. L. and Rickard, D.T.: "Temperature Dependence of Calcite Dissolution Kinetics between 1 and 62°C at pH 2.7 to 8.4 in Aqueous Solutions." *Geochim. Cosmochim. Acta*, (1987), **48**, 485-493.
34. Lichtner, P. C., et al.: "Reactive Transport in Porous Media," in: *Reviews in Mineralogy*. Lichtner, P.S. and Oelkers, E.H, eds., (1996).
35. Folk, R. L.: "Spectral Subdivision of Limestone." *Amer. Assoc. Petrol. Geol. Mem.*, (1962), **1**, 62-84.
36. Stumm, W.: *Chemistry of Solid Water-Interface*, (1992), New York, Wiley.
37. Arvidson, R. S. and Lutge, A.: "Vertical Scanning Interferometry; the Holy Grail of Low Temperature Dolomite Precipitation Kinetics," *Geological Society of America, 2000 Annual Meeting Abstracts with Programs - Geological Society of America*, (2000) **32**, 7, 79.
38. Land, L. S.: "Failure to Precipitate Dolomite at 25 Degrees C from Dilute Solution Despite 1000-Fold Oversaturation after 32 Years. Geochemistry of Low Temperature Processes," *Aquatic Geochemistry*, (1998), **4**, 3-4, 361-368.

39. Lith, Y.V and Warthmann, R.: "Role of Sulfate Reducing Bacteria during Microbial Dolomite Precipitation as Deduced from Culture Experiments," Journal of Conference, *Cambridge Publications*, (2000), Sept. 3-8, **5**(2), 1038.
40. Wolery, T.J.: "EQ3NR, A Computer Program for Geochemical Aqueous Speciation-Solubility Calculations: User's Guide and Documentation" UCRL-53414, Lawrence Livermore National Laboratory, (1983).
41. Grigg, R.B. and Svec, R.K.: "Co-injected CO<sub>2</sub>-Brine Interactions with Indiana Limestone," prepared for presentation at the 2003 Symposium of The Society of Core Analysts, 21-24 September, Pau, France